Mon. Not. R. Astron. Soc. **000**, 1–11 (2003) Printed 2 February 2008 (MN LATEX style file v1.4)

Correlated Optical and X-ray Variability in LMC X–2

K.E. McGowan[1,2⋆], P.A. Charles[2,3], D. O'Donoghue[4], A.P. Smale[5]

[1] *Los Alamos National Laboratory, MS D436, Los Alamos, NM 87545, USA*
[2] *Department of Physics, University of Oxford, Oxford OX1 3RH*
[3] *Department of Physics & Astronomy, University of Southampton, Southampton S017 1BJ*
[4] *South African Astronomical Observatory, PO Box 9, Observatory 7935, Cape Town, South Africa*
[5] *Laboratory for High Energy Astrophysics, Code 662, NASA/Goddard Space Flight Center, Greenbelt, MD 20771, USA*

2 February 2008

ABSTRACT

We have obtained high time resolution (seconds) photometry of LMC X–2 in December 1997, simultaneously with the Rossi X-ray Timing Explorer (*RXTE*), in order to search for correlated X-ray and optical variability on timescales from seconds to hours. We find that the optical and X-ray data are correlated only when the source is in a high, active X-ray state. Our analysis shows evidence for the X-ray emission leading the optical with a mean delay of < 20 s. The timescale for the lag can be reconciled with disc reprocessing, driven by the higher energy X-rays, only by considering the lower limit for the delay. The results are compared with a similar analysis of archival data of Sco X–1.

Key words: binaries: close - stars: individual: LMC X–2, Sco X–1 - X-rays: stars

1 INTRODUCTION

LMC X–2 is the most X-ray luminous low mass X-ray binary (LMXB) known. It was first observed in early satellite flights (Leong et al. 1971) and observations showed it to vary from $L_X \sim 0.6$–3×10^{38} erg s^{-1}(Markert & Clark 1975; Johnston, Bradt & Doxsey 1979; Long, Helfand & Grabelsky 1981). Using a precise X-ray location Johnston et al. (1979) LMC X–2 was optically identified as a faint, $V \sim 18.8$, blue star (Pakull 1978; Pakull & Swings 1979).

X-ray light curves from *EXOSAT* (Bonnet-Bidaud et al. 1989) showed that the source was most variable in the highest energy range (3.6–11 keV), the variability decreased with energy and it was almost constant in the lowest energy range (0.9–2.4 keV). LMC X–2 displayed flaring activity which was characterized by a spectral hardening above an energy of ∼3.6 keV.

The optical spectrum is that of a typical LMXB with weak Hα, Hβ and HeII λ4686 emission superimposed on a blue continuum. The characteristics of the optical spectrum, the relatively soft X-ray spectrum, and the high X-ray to optical luminosity ($L_X/L_{opt} \sim 600$), imply LMC X–2 is similar to galactic LMXBs (e.g. van Paradijs 1983). The optical spectrum lacks the Bowen blend, but this is probably due to the lower metal abundances in the LMC (Johnston, Bradt & Doxsey 1979), which is also used to account for the exceptionally high X-ray luminosities of the LMC X-ray binaries (Motch & Pakull 1989). LMC X–2's similarity to LMXBs in the Galaxy suggested a likely short orbital period (i.e. $\lesssim 1$ d).

However, in spite of a number of studies, the period of LMC X–2 remains uncertain. Motch et al. (1985) and Bonnet-Bidaud et al. (1989) found evidence for a period of ∼ 6.4 h, whereas Callanan et al. (1990) found a periodicity of 8.15 h, and Crampton et al. (1990) suggested a much longer period of ∼ 12.5 days. The only previous simultaneous optical and X-ray coverage of LMC X–2 was very short (6 h) and showed no correlation between the two light curves (Bonnet-Bidaud et al. 1989). Here we present the results of much more extensive simultaneous optical and X-ray photometry of LMC X–2 from December 1997, the aim of which was to search for correlated X-ray and optical variability on timescales from seconds to hours and to investigate the previously claimed periodicities.

2 OBSERVATIONS AND DATA ANALYSIS

Observations of the optical counterpart of LMC X–2 were performed using the UCT–CCD fast photometer (O'Donoghue 1995) at the Cassegrain focus of the 1.9 m telescope at SAAO, Sutherland on 1997 December 4–6. The UCT–CCD fast photometer is a Wright Camera 576 × 420 coated GEC CCD, which was used half-masked so as to operate in frame-transfer mode. In this configuration, only half of the chip is exposed, and at the end of the integration the

⋆ email: mcgowan@lanl.gov

Table 1. Log of high-speed photometry observations of LMC X–2 : SAAO 1.9 m.

Start Time JD +2450000	Duration (hr)	Exposure Time (s)
787.306	0.70	2
787.355	1.35	2
787.425	0.87	5
787.510	0.95	2
787.558	0.58	2
788.306	0.23	2
788.423	1.35	10
788.490	0.57	10
789.286	0.45	2
789.315	0.57	2
789.422	1.42	2
789.489	0.53	2
789.558	0.27	2

signal is read out through the masked half. In this way, it is possible to obtain consecutive exposures of as short as 1 s with no deadtime. White light high-speed photometry runs were carried out with integration times of 2–10 s (see Table 1).

As the seeing fluctuated during the observations, point spread function (PSF) fitting was essential to obtain good photometry. The reductions were performed with the IRAF implementation of DAOPHOT II (Stetson 1987). For our purposes only the relative brightness of a star is of importance, and so differential photometry was applied to help reduce the effects of any variations in transparency, employing 2 bright local standards within our field of view. This resulted in a relative precision of ± 0.04 mag per frame.

The X-ray data were obtained using the proportional counter array (PCA) instrument on the *RXTE* satellite between 1997 December 2 18:52 UT and December 7 1:40 UT, in an observing strategy designed to achieve the maximum amount of simultaneous coverage with the optical photometry. Data from all proportional counter unit (PCU) layers and detectors were included in the creation of X-ray light curves in the 2–10 keV energy range. We chose a time resolution of 1 s, rather than the standard 16 s, for cross-correlation purposes. Background subtraction was performed utilising standard models generated by the *RXTE*/PCA team. Further information about the X-ray observations can be found in Smale & Kuulkers (2000).

Optical data simultaneous with the *RXTE* data were obtained covering 6.6 h, 4.68 h, and 6.8 h respectively on the three optical observing nights (see Fig. 1). The timing of the X-ray data was measured in Julian Date (Terrestrial Time) [JD(TT)]. The optical timing was measured in JD(UT) and had to be corrected for the accumulated leap seconds to produce timings in JD(TT) (see XTE Time Tutorial†).

Although the UCT–CCD running in frame transfer mode can take exposures as fast as 1 s, we found that the computer used to store the images had a limit on how fast it could transfer the data. Hence, the effective exposure time for the shortest observations is 2.019 s.

† http://legacy.gsfc.nasa.gov/docs/xte/abc/time_tutorial.html

The X-ray data has a time resolution of 1 s, the optical data 2–10 s. Visual examination of the light curves shows that the variability in both is on timescales of greater than many tens of seconds. Hence we found this variability to be displayed most clearly when both X-ray and optical data were binned into 16 s intervals (Fig. 2). However, to quantitatively study the correlation between the two, and to search for any delays between the two wavebands, we binned the X-ray light curve onto the corresponding optical light curve time bins i.e. 2, 5 or 10 s (see Table 1).

3 LMC X–2 TEMPORAL ANALYSIS

LMC X–2 exhibits clear night-to-night variations of several tenths of a magnitude, fine structure within each night is also evident (Fig. 1). The intervals of optical photometry are too short to allow detection of the previously quoted orbital periods of 8.15 h and 12.5 d. Furthermore, a period search on the dataset failed to reveal any consistent shorter term periodicities in the data.

In order to investigate the correlation between the optical and X-ray data, to determine whether a delay is present and to quantify this delay we performed (i) a cross-correlation analysis, and (ii) modelling of the optical light curve by convolving the X-ray light curve with a Gaussian transfer function.

3.1 Cross-correlation

We performed the cross-correlations of each run of optical and X-ray data by employing a modified version of the Interpolation Correlation Function, ICF (Gaskell & Peterson 1987; Hynes et al. 1998). As our optical and X-ray data are binned onto the same time resolution, and we edited the lengths of the two time series to be the same, interpolation is not required. The cross-correlation technique that results is effectively a Discrete Correlation Function, DCF, similar to that of Edelson & Krolik (1988). We also implemented code based on standard cross-correlation function (CCF) routines which are again similar to a DCF; both the ICF and CCF methods agree well.

Concerns have been raised in the literature (see Koen 1994) about the validity of cross-correlation as a means to finding lags within wavebands for a source due to the effects of the auto-correlation function in the individual time-series on the CCFs produced. This can lead to the peak in the CCF being shifted from its true value.

For the one simultaneous run (JD 2450787.355 – 2450787.406) where LMC X–2 is seen to be in a bright, active X-ray state (i.e. flares are present and the mean PCA count rate in the 2–10 keV light curve is 400 counts/s) a broad peaked CCF is produced. For this run the resulting time bins are of 2.019 s. The position of the CCF peak indicates there is a non-zero delay of order ~ 20 s between the two datasets. The sign convention of the CCF implies that the optical lags the X-rays (Fig. 3). This is expected if the delay is attributed to the X-rays heating some part of the binary system which in turn produces optical emission. The standard deviation for the CCF for uncorrelated data is given by $\sigma_n = 1/(n-2)^{1/2}$, where n is the number of observed points (Gaskell & Peterson 1987). However, this is

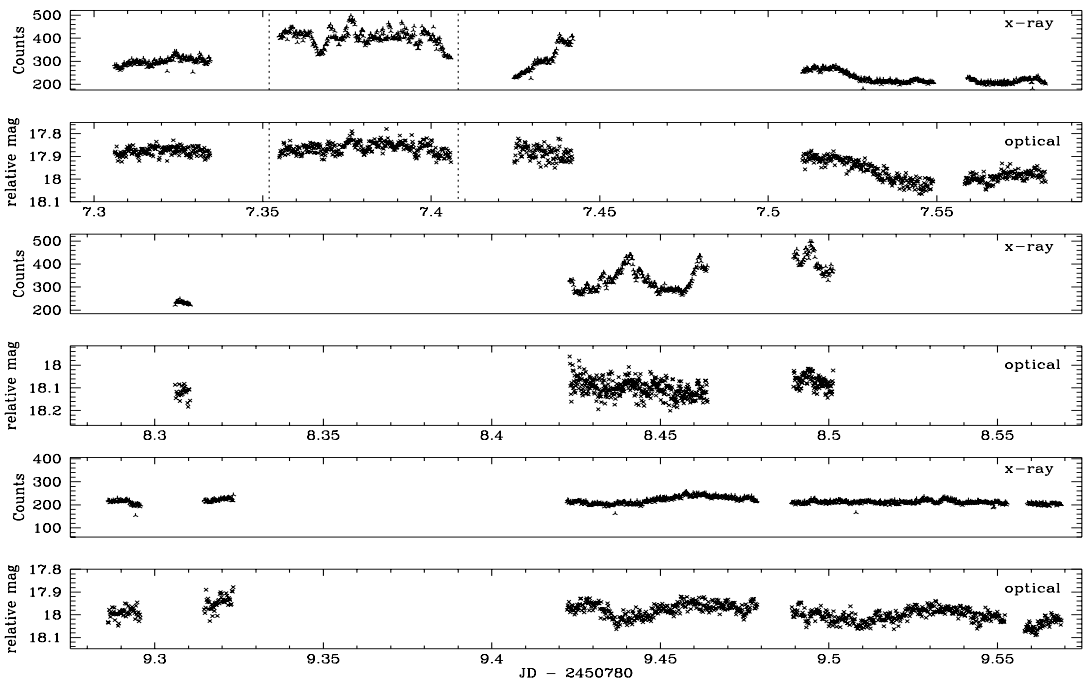

Figure 1. All simultaneous SAAO optical (white light) and *RXTE*/PCA X-ray data of LMC X–2 taken over the period 1997 December 4–6. The vertical dotted lines indicate the run in which correlated variability is found (see Section 3 and Fig. 2).

only valid for data with no autocorrelation. We therefore use the results from Koen (2003) in which the standard errors on the CCF are determined by fitting standard parametric times series models to the data. In all other runs the X-rays were in a low state (with mean PCA count rate for the 2–10 keV light curve < 400 counts/s) and no significant peaks in the CCFs are found.

As noted above, although the X-ray light curves have an intrinsic 1 s time resolution, the data generated by the background subtraction models for the X-ray light curve have a time resolution of 16 s. In order to determine whether or not the background model is contributing to the delay in the CCF, non-background subtracted X-ray data were also used. We detrended these data to reduce the long-term effects of the changing background before the cross-correlation analysis was performed. We find a broad peak in the CCF with similar values as previously, indicating that the lag we find is not due to the background subtraction procedure.

To calculate a mean value for the range of delays found for LMC X–2, and to investigate its significance, we performed Monte Carlo simulations to create simulated optical and X-ray light curves. The simulated data were produced by sampling a Gaussian random number generator with a mean value equivalent to the average of the entire real dataset, and a sigma equal to the error bar on each individual real point. Employing this method we calculated new values for each observed optical and X-ray data point. The simulated datasets were cross-correlated with each other exactly as for the real data. To produce good statistics, this was repeated ten thousand times. Statistics were computed on the spread of values obtained giving a mean of 14.2 s and a standard deviation of 8.7 s. This value represents the typical time lag for these data, however, a typical lag of zero is not excluded at the level of twice the standard deviation. A zero delay is *not* ruled out as there *are* times when there is *no* lag, and we expect it to be modulated on the orbital period. Hence the quoted error ($\pm$8.7 s) is *not* the true error on the mean delay, but more an indication of the range over which the lags are seen. We note that this method leads to there being no correlation between each set of simulated optical and X-ray data. Therefore we have a measure of the spread of correlations that can occur due to chance when there is no real correlation between the two datasets. A much more detailed study of the statistical properties of cross-correlating limited datasets with variable binning is presented by Koen (2003), in an analysis which uses some of these data of LMC X–2 as an example. As for the standard analysis we use here, Koen (2003) concludes that there is strong evidence for variable X-ray/optical lags, but is able to demonstrate the level of statistical significance much more clearly.

To study the effect of the flaring behaviour in the 2–10 keV X-ray light curve we cross-correlated 1000 s sections of the optical and X-ray data as above. The CCFs produced (Fig. 4) demonstrate well that correlated variability is only seen when there is high X-ray activity. The first three panels (0–2000 s) in Fig. 4 show the effect that the large dip in the X-ray light curve has on the correlated variability (which is to produce the longer lags). The other panels (1500–4500 s) which have no contribution from the dip show much narrower CCFs.

We also investigated the source of the flaring activity

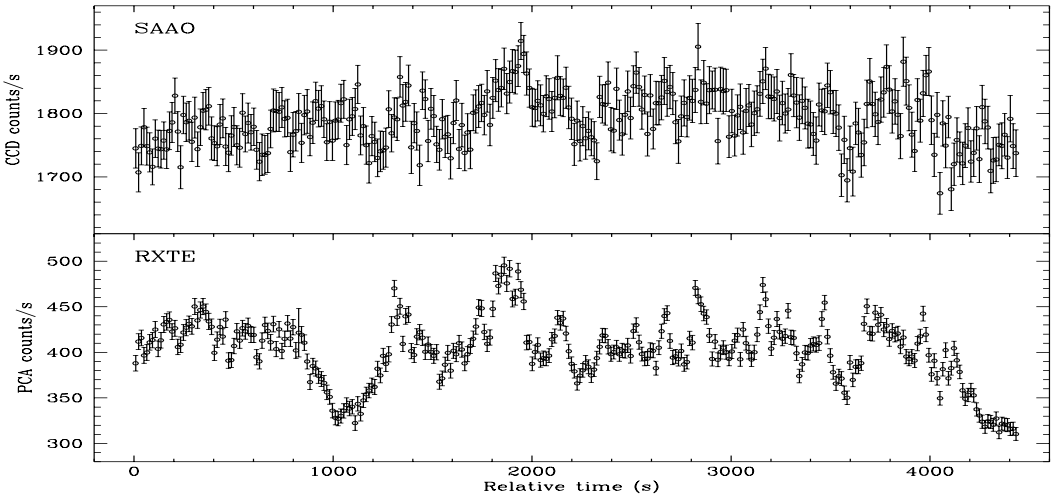

Figure 2. The optical (top) and X-ray (bottom) light curves of LMC X–2 for the run in which correlated variability is found, taken 1997 December 4. Both light curves have been binned on 16 s.

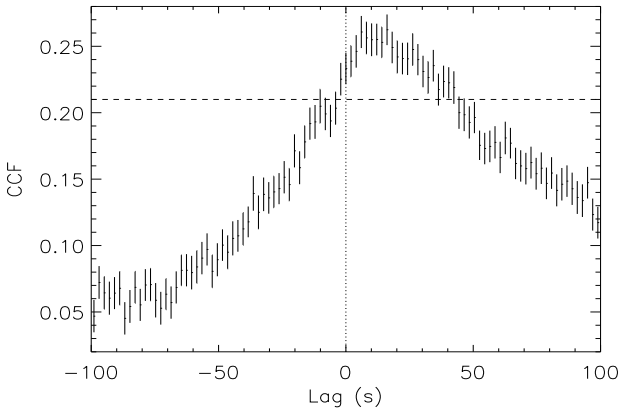

Figure 3. Cross-correlation function for LMC X–2. Sign convention is such that positive lags correspond to X-rays leading the optical. The dashed line shows the 3σ significance level of the CCF from the standard errors (see Koen 2003).

observed in the X-ray light curve. We extracted data in the soft (2–4 keV) and hard (4–10 keV) energy ranges (see Section 2). The light curves were cross-correlated with the optical data as before. The hard and soft X-ray light curves are shown in Fig. 5 (left). The light curves clearly demonstrate that LMC X–2 is most variable at hard energies with little activity in the soft energies, as has been noted by Bonnet-Bidaud et al. (1989). The CCFs for both light curves are shown in Fig. 5 (right). We note that there are less counts in the soft X-ray light curve than the hard X-ray light curve which could be responsible for the lack of a significant peak in the CCF for the soft band. However, we find that in the hard light curve the feature at ~ 1800 s has a $\sim 16\%$ excess compared to the mean, while in the soft light curve it is an excess of only $\sim 5\%$. This indicates that the features which lead to the CCF peak in the hard band are not present in the soft energies. The large dip is present in both the hard and soft light curves.

The measurement of the cross-correlation function provides a characteristic delay which does not depend on particular model fitting. To characterize the distribution of time delays present between the optical and X-ray light curves we modelled the data with a transfer function.

3.2 Transfer Function

In order to model the time lag between the optical and X-ray data of LMC X–2 we predict the optical light curve by convolving the observed X-ray light curve with a Gaussian transfer function. We use χ^2 fitting to obtain the best-fit to the optical light curve (see Hynes et al. 1998; Kong et al. 2000). The Gaussian transfer function is given by

$$\psi(\tau) = \frac{\Psi}{\sqrt{2\pi\Delta\tau}} e^{-\frac{1}{2}\left(\frac{\tau-\tau_0}{\Delta\tau}\right)^2}, \quad (1)$$

where τ_0 is the mean time delay, and $\Delta\tau$ is the dispersion or root-mean-square time delay, which is a measure of the

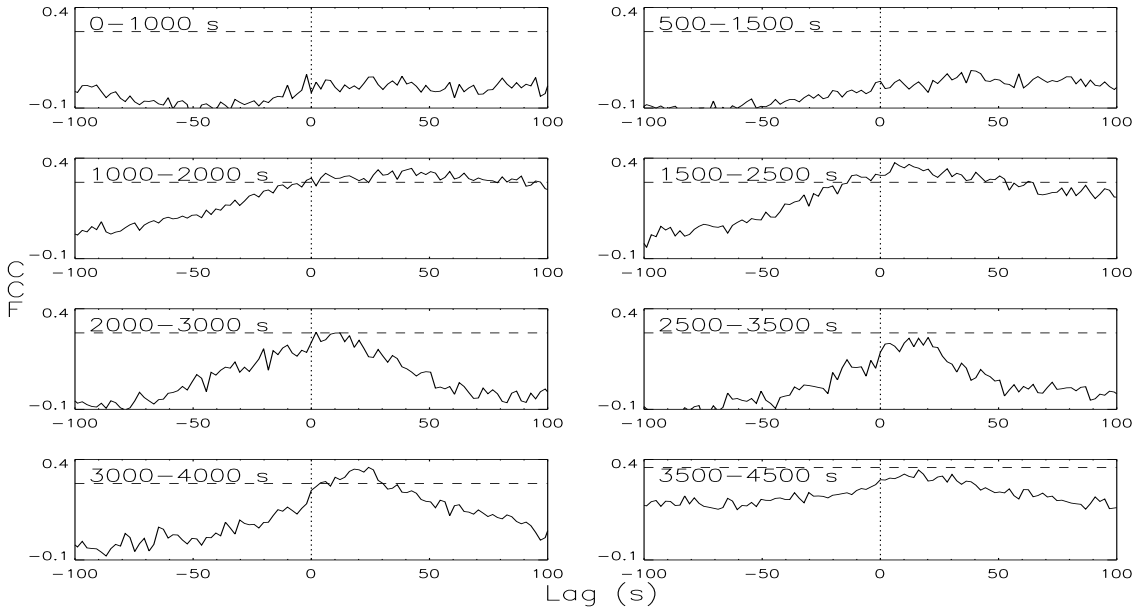

Figure 4. Cross-correlation functions for 1000 s sections of optical and X-ray data of LMC X–2. Sign convention is such that positive lags correspond to X-rays leading the optical. The dashed lines show the 2σ significance level of the CCF from the standard errors (see Koen 2003).

Table 2. Summary of results from convolution of a Gaussian transfer function to the three different X-ray energy band light curves of LMC X–2.

	2–10 keV	4–10 keV
τ_0 (s)	$18.6^{+7.4}_{-6.6}$	$14.7^{+7.3}_{-5.7}$
$\Delta\tau$ (s)	$10.2^{+5.8}_{-5.7}$	$9.0^{+7.0}_{-4.5}$
$\Psi(10^{-3})$	10.8	13.4
χ^2_ν	0.71	0.69

width of the Gaussian, and is equivalent to the degree of 'smearing'. The strength of the response is given by Ψ.

We performed a series of convolutions of the transfer function with the X-ray light curve in the 2–10 keV and 4–10 keV energy bands, varying both τ_0 and $\Delta\tau$ independently. Table 2 summarizes the results of fitting Gaussian transfer functions to the two X-ray light curves. Fig. 6 shows the best-fitting predicted light curves from the convolutions superimposed on the optical light curve of LMC X–2. We did not perform this analysis with the soft (2–4 keV) X-ray data due to the lack of variability in the light curve (see Section 3.1).

The values for χ^2_ν are good for both bands. The principal features of the optical light curve are reproduced well in the predicted light curves from the 2–10 keV and 4–10 keV energies.

The mean delay and dispersion between the optical and 2–10 keV X-ray data are 18.6 and 10.2 s respectively, for the 4–10 keV data the mean delay and dispersion are 14.7 and 9.0 s. The errors on the mean delay values indicate that a non-zero lag is present at the 2.8σ and 2.6σ levels for the 2–10 keV and 4–10 keV bands. The strength of the response is an indication that a greater proportion of the reprocessing is driven by higher energies.

4 COMPARISON WITH SCO X–1

It is instructive to compare LMC X–2's behaviour with that of the brightest galactic LMXB, Sco X–1. Ilovaisky et al. (1980; hereafter I80) studied the correlation of variability in simultaneous optical and X-ray observations of Sco X–1 using *SAS-3*, *Copernicus* and conventional photoelectric photometry. As we have found with LMC X–2, I80 only detected correlated variability occurring when the source was in a bright, active X-ray state (Fig. 7), with the correlation decreasing as Sco X–1 became less active. More interestingly, they also found that the peak in their cross-correlation curve gave a delay which was consistent with the optical being delayed with respect to the X-rays. They attributed this delay to reprocessing of the X-rays in the binary system. From their observations during a period of high activity they suggested that the optical features were delayed by ~ 30 s compared with those in the X-rays. From their cross-correlation analysis for those data when Sco X–1 was in an active state they found a range of values for the delay from a few seconds to a few tens of seconds. The peak value for the cross-correlation function (CCF) at these delays was not much greater than that for zero lag and so they concluded that the delays were not very significant.

Petro et al. (1981; hereafter P81) also found correlated variability in Sco X–1. Their analysis suggested an optical smearing timescale ('filter' or 'processing' time) of ~ 20 s, describing the optical flares as 'filtered' versions of the X-ray flares. They concluded that the delay could not be due to reprocessing on the secondary as this required a timescale of only ~ 10 s, and therefore could not explain the presence of the long smearing timescale for the system. From the rise times of the correlated optical and X-ray flares they also concluded that the reprocessing site that produced the optical flares must be in a different region from the site of X-ray production (c.f. Pedersen et al. 1982).

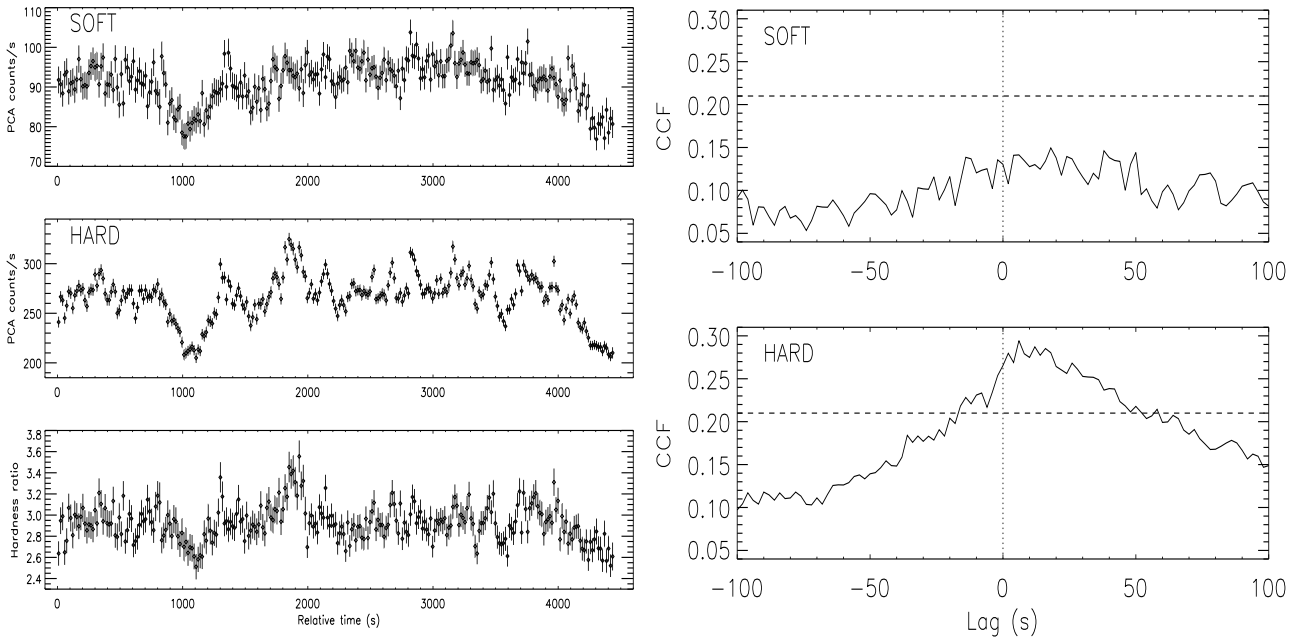

Figure 5. Left panels, soft (2–4 keV) (first) and hard (4–10 keV) (second) X-ray light curves of LMC X–2, hardness ratio (third), defined as (hard)/(soft). Right panels, the CCFs for the soft (first) and hard light curves (second). Sign convention is such that positive lags correspond to X-rays leading the optical. The dashed lines show the 3σ significance level of the CCF from the standard errors (see Koen 2003).

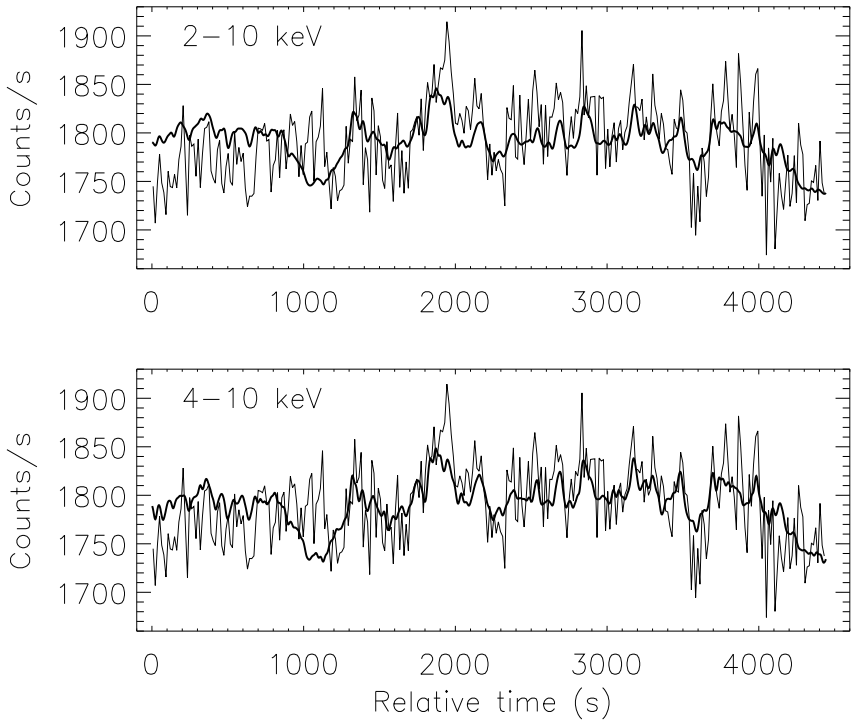

Figure 6. Best-fitting predicted light curves (thick line) using a Gaussian transfer function on the two X-ray bands of LMC X–2, 2–10 keV (top) and 4–10 keV (bottom). The resulting curves are superimposed on the optical light curve which has been binned on 16 s for clarity.

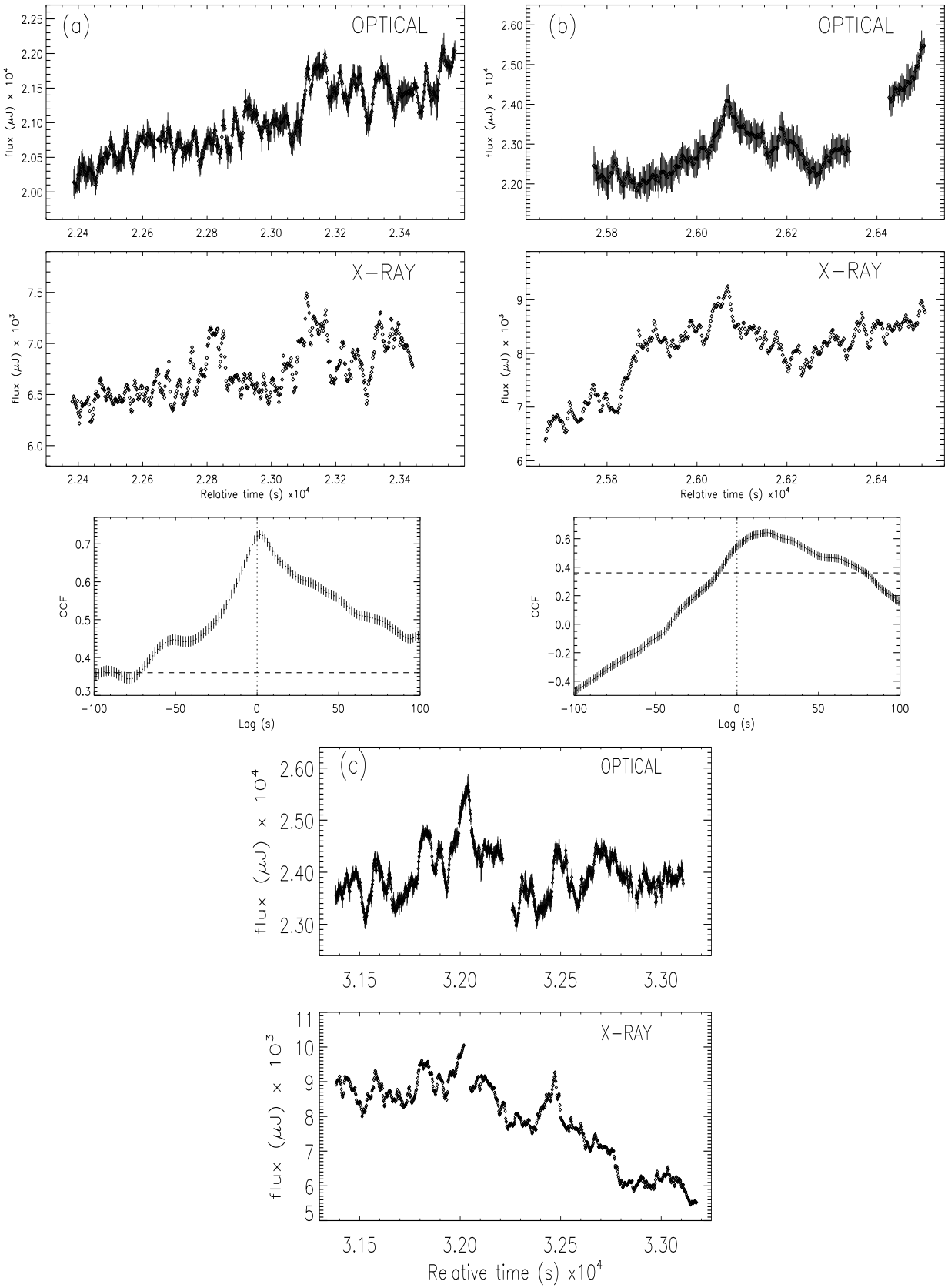

Figure 7. (a), (b), (c) Simultaneous optical and *SAS-3* X-ray active state data of Sco X–1 taken on 1977 March 15 (Ilovaisky et al. 1980). The lower panels in (a) and (b) show the CCFs for these two datasets. All light curves are binned on 2 s resolution. The dashed lines in the CCFs in (a) and (b) show the 3σ significance level of the CCF from the standard errors (see Koen 2003).

Following our analysis above of LMC X–2, we decided to investigate such previous X-ray/optical observations of LMXB's in greater detail.

4.1 Cross-correlation

We digitized the active state optical and X-ray data of Sco X–1 from I80, converting the data to μJy. We then performed cross-correlations of the simultaneous data as have been done for LMC X–2 (Fig. 7). We find that the delays for the first two sets of data are $\sim 1.7\pm0.9$ s and 17.6 ± 5.4 s. The significance of both CCF peaks is $> 4\sigma$. The results indicate that a lag of zero is not ruled out at the 2σ level for the first set of data, for the second set there is $> 3\sigma$ confidence of a non-zero lag. For the third set of data no significant delay is found, but note the decline in the X-rays compared to the constant optical. The lack of a delay for the second half of the data demonstrates again that the X-rays must be in an active state (i.e. with flaring) to show correlated variability with the optical data.

We cross-correlated the two simultaneous active state datasets from P81, finding delays of 5.9 ± 2.5 s and 5.7 ± 2.8 s (Fig. 8). There is evidence for a non-zero lag in both datasets at the $> 2\sigma$ level.

As in LMC X–2, Sco X–1 exhibits an increase in correlation between the optical and the X-rays as the source becomes more active. I80 suggested that this could be due to either one or two regions of optical emission. In the case of one optical emitting zone, they suggested that the optical reprocessing region is illuminated by the X-ray source at all times, but 'something' is required to damp out the X-ray variability between the compact object and the observer when the source is in a non-active state, or perhaps the optical "region" cannot then see the X-rays. For the case of two emitting regions, they suggest that the uncorrelated emission ($\sim$ 25% less energetic in the X-rays than during correlated emission) could be due to optical emission from the disc itself, while the correlated emission could be due to X-ray heating of different parts of the system and would be directly related to the X-ray emission.

The lags determined from the cross-correlation analysis again represent the characteristic delay present between the optical and X-ray light curves. In order to model the time delay we have also convolved the X-ray light curves of Sco X–1 from I80 and P81 with a Gaussian transfer function, as has been done for LMC X–2 (see Section 3.2).

4.2 Transfer Function

A series of convolutions of the transfer function with each of the X-ray light curves were performed on the first two datasets from I80 (Fig 7 (a) and (b)), and both sets of data from P81 (Fig 8 (a) and (b)). Again both τ_0 and $\Delta\tau$ were varied independently. The results of fitting the Gaussian transfer functions to the Sco X–1 X-ray data are summarized in Table 3. The values of χ^2_ν indicate that the fits are not good. The best-fitting predicted light curves from the convolutions superimposed on the optical light curves are shown in Fig 9.

The predicted light curves reproduce the optical data marginally for the first set of I80 data and the first set of P81 data (Fig 9, (a) and (c)). For the second sets of data from I80 and P81 (Fig 9, (b) and (d)) only the overall shape of the optical light curves are reproduced, and not the small scale features. The results for the first datasets of I80 and P81 suggest non-zero lags of 1.6 and 8.0 s respectively, and are present with 3.2σ and 10σ confidence, respectively.

Table 3. Summary of results from convolution of a Gaussian transfer function to the X-ray light curves of Sco X–1.

	Ilovaisky (a)	Ilovaisky (b)	Petro (a)	Petro (b)
τ_0 (s)	$1.6^{+0.6}_{-0.5}$	$42.0^{+2.5}_{-3.0}$	8.0 ± 0.8	$21.9^{+5.1}_{-4.9}$
$\Delta\tau$ (s)	$4.9^{+0.8}_{-0.7}$	$82.0^{+5.0}_{-4.0}$	8.6 ± 1.3	$16.8^{+4.2}_{-3.8}$
$\Psi(10^{-3})$	5.27	5.30	74.7	13.8
χ^2_ν	4.00	4.05	2.98	3.69

5 DISCUSSION

We find evidence that the optical emission of LMC X–2 is delayed with respect to the X-ray emission. The presence of a non-zero delay has $> 2.6\sigma$ confidence. If the lag is greater than zero, reprocessing of the X-rays in material at some distance from the X-ray source could be responsible. Potential candidates as reprocessing regions include the outer areas of the accretion disc and the heated face of the secondary star. However, to determine where the reprocessing is occurring requires a detailed knowledge of the binary system parameters. These same *RXTE* observations have provided a possible new confirmation of the 8.2 h orbital period in the X-ray data (Smale & Kuulkers 2000), but the nature of the compact object remains obscure. Assuming that 8.2 h is indeed the orbital period (see also Alcock et al. 2000), then the compact object could either be :

(a) a neutron star, assumed mass $1.4M_\odot$ in which case the tidal disc radius will be $\sim 1R_\odot$ (equiv. 2–3 s light travel time) and the secondary at a distance $\sim 2.5R_\odot$ ($\sim$ 6 s); or (b) a $10M_\odot$ black hole with disc radius $\sim 2R_\odot$ ($\sim$ 4–5 s) and separation of the secondary $\sim 5R_\odot$ ($\sim$ 11 s). [Note, however, that if the period were to be 12.5 d, then these delays would be (a) 25–28 s and > 60 s (b) 47–54 s and > 117 s].

The light travel times arise from the time of flight differences for emission that is observed directly and emission which is reprocessed and re-emitted before travelling to the observer. The maximum delay is twice the binary separation, plus any time due to reprocessing/diffusion. Our results for the optical and 2–10 keV X-ray data of LMC X–2 give a mean lag of $18.6^{+7.4}_{-6.6}$ s and a distribution of $10.2^{+5.8}_{-5.7}$ s. The 2σ lower limit for the lag is 5.4 s. Employing the period and ephemeris given in Smale & Kuulkers (2000), the phase at the beginning of the correlated optical and X-ray observations of LMC X–2 is 0.4, where $\phi = 0$ corresponds to the time of minimum light. Lags of greater than 6 s would be expected for this phase if the secondary star is the reprocessing site, thus the 2σ lower limit for the lag may be reconciled with disc reprocessing.

The light travel times for the disc and the secondary star in Sco X–1, given its known orbital period of 18.9 h (Gottlieb, Wright & Liller 1975; LaSala & Thorstensen 1985),

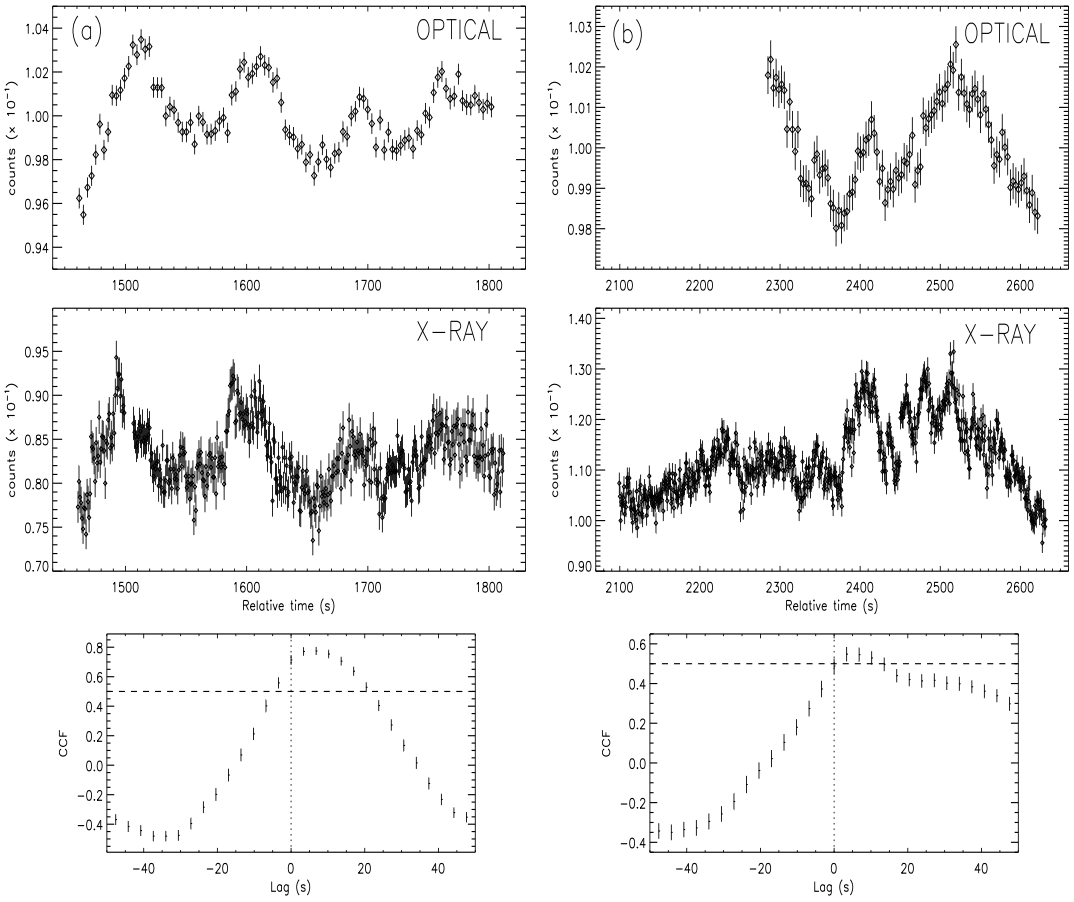

Figure 8. (a), (b) Simultaneous optical and X-ray active state data of Sco X–1 taken on 1979 March 8 (Petro et al. 1981). The lower panels show the CCFs for these two datasets. The dashed lines in the CCFs show the 2σ significance level of the CCF from the standard errors (see Koen 2003).

are 4–5 and 10 s respectively. Note that the secondary has never been detected in Sco X–1, however QPO have been observed (Middleditch & Priedhorsky 1985) and the delay values given above assume a neutron star compact object. Considering the first sets of Sco X–1 data from I80 and P81, our 2σ lower limits for the lags of 0.6 and 6.4 s from the convolution of the X-ray data with a Gaussian transfer function suggest reprocessing in the disc. However, the goodness of fits are poor, and the transfer function does not work well for the other two sets of Sco X–1 data.

In LMC X–2 and Sco X–1 the delays found from Gaussian modelling and the cross-correlation analysis are in good agreement. It is therefore likely that the non-zero delays determined for the second sets of data from I80 and P81 with the cross-correlation technique are close to the true values. In both cases the lower limit for the lags are consistent with the disc being the site of reprocessing.

Other authors have found delays in optical/X-ray bursts for X-ray binaries in which the optical emission is suggested to be the result of X-ray reprocessing. The optical burst is described as a delayed and smeared version of the X-ray burst, the time delays found being consistent with the reprocessing occurring in the accretion disc (Matsuoka et al. 1984 and references therein; Kong et al. 2000). The time delays found for the bursts are much shorter than those for LMC X–2. However, the X-ray spectra for the bursts are much softer than for LMC X–2, indicating that the delays found for the bursts are due to processes closer to the surface of the disc than we are seeing. We find evidence for time lags when LMC X–2 displays hard flaring behaviour which suggests that the optical is responding to X-rays which have penetrated to a deeper level in the disc.

However, for LMC X–2 and Sco X–1 we are considering the 2σ lower limit for the lags, which implies that our delays could be much longer. In the case of LMC X–2, even the lower limit for the delay is longer than the light travel time of the disc, while shorter than the distance to the secondary. Note that this result is from only one correlated optical and X-ray run.

It is obvious that more data are needed to confirm this result. It would also be instructive to use the technique of O'Brien et al. (2002) in which the time delay transfer functions are modelled by simulating the distribution of the reprocessing regions, employing geometrical and binary parameters. In order to explain the longer than disc crossing times however, more sophisticated radiative transfer models are likely needed. We require some mechanism that can add a finite time to the light travel time to account for the longer delays that may be present. One possible method is to take into account the time component that could be present

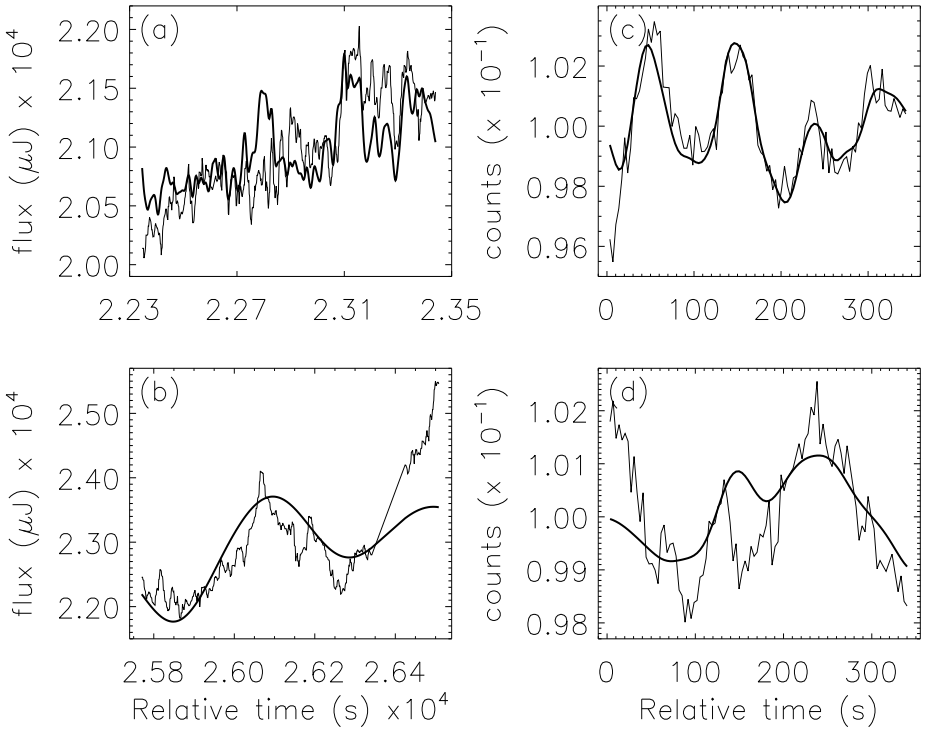

Figure 9. Best-fitting predicted light curves (thick line) using a Gaussian transfer function on the X-ray light curves of Sco X–1 from Ilovaisky et al. (1980) (a), (b) and from Petro et al. (1981) (c), (d). The resulting curves are superimposed on the optical light curves.

due to diffusion. Thus, the delay could be interpreted as the light travel time with an added component due to diffusion within the absorption/re-emission region. Calculations to determine the order of the diffusion timescale using a simplistic, however unrealistic, single temperature atmosphere are presented in Appendix A.

Our observations of LMC X–2 show the first correlated optical and X-ray variability for the source. The temporal analysis provides evidence that the X-rays lead the optical, which implies reprocessing is occurring. We also find that the optical light curves of Sco X–1 are delayed with respect to the X-ray light curves from analysis of archival data. Further observations are needed when LMC X–2 and Sco X–1 are in a bright, active X-ray state to investigate the source of the lags. This could be combined with additional optical observations to study the colours and spectra of the two sources at that time.

6 ACKNOWLEDGEMENTS

We thank Philipp Podsiadlowski and Keith Horne for useful discussions on the reprocessing physics. We also thank Chris Koen, Rob Hynes and Albert Kong for useful comments on the temporal analysis methods.

REFERENCES

Alcock C., et al., 2000, MNRAS, 316, 729
Allen C.W., 1973, Astrophysical Quantities. University of London, Athlone Press, 3rd ed.
Bonnet-Bidaud J.M., Motch C., Beuermann K., Pakull M.W., Parmar A.N., van der Klis M., 1989, A&A, 213, 97
Callanan P.J., Charles P.A., van Paradijs J., van der Klis M., Pedersen H., Harlaftis E.T., 1990, A&A, 240, 346
Crampton D., Cowley A.P., Hutchings J.B., Schmidtke P.C., Thompson I.B., 1990, ApJ, 355, 496
Edelson R.A., Krolik J.H., 1988, ApJ, 333, 646
Gaskell C.M., Peterson B.M., 1987, ApJS, 65, 1
Gottlieb E.W., Wright E.L., Liller W. 1975, ApJ, 195, L33
Harlaftis E.T., Charles P.A., Horne K., 1997, MNRAS, 285, 673
Hynes R.I., et al., 1998, MNRAS, 299, L37
Ilovaisky S.A., et al., 1980, MNRAS, 191, 81, (I80)
Johnston M.D., Bradt H.V., Doxsey R.E., 1979, ApJ, 233, 514
Koen C., 1994, MNRAS, 268, 690
Koen C., 2003, MNRAS, in press
Kong A.K.H., Homer L., Kuulkers E., Charles P.A., Smale A.P., 2000, MNRAS, 311, 405
LaSala J., Thorstensen J.R., 1985, AJ, 90, 2077
Leong C., Kellog E., Gursky H., Tananbaum H., Giacconi R., 1971, ApJ, 170, L67
Lomb N.R., 1976, Astrophys. Space Sci., 39, 447
Long K.S., Helfand D.J., Grabelsky D.A., 1981, ApJ, 248, 925
Markert T.H., Clark G.W., 1975, ApJ, 196, L55
Matsuoka M., et al., 1984, ApJ, 283, 774
Middleditch J., Priedhorsky W., 1985, IAU Circ., 4060
Motch C., Chevalier C., Ilovaisky S.A., Pakull M.W., 1985, Space Sci. Rev., 40, 239
Motch C., Pakull M.W., 1989, A&A, 214, L1
O'Brien K., Horne K., Hynes R.I., Chen W., Haswell C.A., Still M.D., 2002, MNRAS, 334, 426
O'Donoghue D., 1995, Baltic Astron., 4, 519
Pakull M.W., 1978, IAU Circ 3313
Pakull M.W., Swings J.P. 1979, IAU Circ 3318
Pedersen H., et al., 1982, ApJ, 263, 325
Petro L.D., Bradt H.V., Kelley R.L., Horne K., Gomer R., 1981, ApJ, 251, L7, (P81)
Roberts D.H., Lehar J., Dreher J.W., 1987, AJ, 93, 968
Smale A., Kuulkers E., 2000, ApJ, 528, 702

Stetson P.B., 1987, PASP, 99, 191
van Paradijs J., 1983, in Accretion-Driven Stellar X-ray Sources, ed. Lewin, van den Heuvel, 189, Cambridge University Press, Cambridge
Webbink R.F., Rappaport S., Savonije G.J., 1983, ApJ, 270, 678
White N.E., 1989, Astron. Ast. Rev., 1, 85

APPENDIX A: DIFFUSION TIMESCALE CALCULATIONS

Using a simple model for the secondary star or the 'atmosphere' of the disc, we can estimate the duration of the diffusion timescale, the time it takes for the X-ray photons to be absorbed and the energy deposited there to be re-emitted in the optical. This timescale is heavily dependent on the density and opacity of the star/disc.

Assume the X-rays penetrate to a depth d in the photosphere where κ_x is X-ray opacity ($\kappa_x = 0.2(1+X) \sim 0.34$ cm^{2}g^{-1}) and ρ is density, then

$$d \sim \frac{1}{\kappa_x \rho} \tag{A1}$$

The number of scatterings is then $\sim (d\kappa_\circ\rho)^2$ where $\kappa_\circ$ is the optical opacity, and the time between each scattering is $\sim 1/(\kappa_\circ\rho c)$. Combining these with Eq. A1 we can define the diffusion timescale as

$$t_{diff} = \left(\frac{\kappa_\circ}{\kappa_x}\right)^2 \cdot \frac{1}{\kappa_\circ \rho c} \tag{A2}$$

From the equations for the optical depth and pressure of the photosphere, assuming that $\kappa_\circ$ is constant in depth d, and that the gravity g remains roughly constant over d, then we can derive an expression for $\kappa_\circ$ (assuming an ideal gas)

$$\frac{\kappa_\circ}{g} = \frac{\frac{2}{3}}{\frac{k}{\mu_H m_H}\rho T_{eff}} \tag{A3}$$

Replacing g in Eq. A3 with GM/R^2 and rearranging to get an expression for $\kappa_\circ\rho$ we can substitute this into Eq. A2 to give

$$t_{diff} = \left(\frac{\kappa_\circ}{\kappa_x}\right)^2 \cdot \left[\frac{\frac{3}{2}\cdot\frac{kT_{eff}}{\mu_H m_H}}{\frac{GM}{R}} \cdot \frac{R}{c}\right] \tag{A4}$$

By calculating the irradiating flux (F_x) we can derive the irradiation temperature T_x, given by

$$T_x = \left(\frac{fF_x}{2\sigma}\right)^{1/4} \tag{A5}$$

where f is 5–10% and σ is the Stefan-Boltzmann constant. Taking T_{eff} in Eq. A4 to be the irradiation temperature, and calculating values for the radius and mass of the secondary in LMC X–2, we find a value of $\sim 6\times10^{-3}$ s for the expression in square brackets in Eq. A4. Using the quoted values for the gravity and density of a K star (Allen 1973) a diffusion time of greater than 20000 s is found (Table A1). As we are trying to calculate the diffusion time for the heated secondary we should use the gravity of a K star, but the density of a B star (e.g. the 5.2 h LMXB X 1822-371 has a low mass secondary but the heated face shows a $\sim$ B star spectrum, Harlaftis, Charles & Horne 1997). For illustrative purposes we use a canonical B star density (Allen 1973) to give an estimate for the diffusion time, resulting in $t_{diff} \sim 1$ s. Table A1 illustrates how the optical opacity is heavily dependent on the density of the star, and in turn how this greatly effects the estimated value for the diffusion time that results. Detailed modelling is required to calculate the diffusion time for the disc. These calculations could assume a spectral-type of $\sim$ A0 for the disc, and would need to take into account the angle of incidence of the incoming radiation and the gravity and density of the disc.

Table A1. Diffusion times for different spectral types.

Spectral Type	log N (cm^{-3})	$\kappa_\circ$	t_{diff} (s)
B0	15.0	4.1	1
A0	15.2	6.6	2
F0	16.1	48.4	117
G0	16.9	331.8	5524
K0	17.2	667.3	22344
M0	17.5	1279.3	82120